ORIGINAL ARTICLE

Polymeric worm-like nanomicellar system for accelerated wound healing

Aarti Singh[1], Adeeba Shakeel[2], Dakshi Kochhar[1,3], Sampathkumar Jeevanandham[1,4], Satyendra Kumar Rajput[5], Monalisa Mukherjee[1,3]

[1]Amity Institute of Click Chemistry Research and Studies, Amity University, [3]Amity Institute of Biotechnology, Amity University, [4]Amity Institute of Nanotechnology, Amity University, [5]Amity Institute of Pharmacy, Amity University, Noida, Uttar Pradesh, [2]All India Institute of Medical Sciences, New Delhi, India

J. Adv. Pharm. Technol. Res.

ABSTRACT

Self-assembly is an unparalleled step in designing macromolecular analogs of nature's simple amphiphiles. Tailoring hydrogel systems – a material with ample potential for wound healing applications – to simultaneously alleviate infection and prompt wound closure is vastly appealing. The poly (DEAEMA-co-AAc) (PDEA) is examined with a cutaneous excisional wound model alterations in wound size, and histological assessments revealed a higher wound healing rate, including dermis proliferation, re-epithelialization, reduced scar formation, and anti-inflammatory properties. Moreover, a mechanism for the formation of spherical and worm-like micelles (WLMs) is delineated using a suite of characterizations. The excellent porosity and ability to absorb exudates impart the PDEA with reliable wound healing. Altogether, this system demonstrates exceptional promise as an infection-mitigating, cell-stimulating, homeostasis-maintaining dressing for accelerated wound healing. The aim and objective of this study is to understand the mechanism of self-assembly in synthesized WLMs from PDEA and their application in wound healing.

Key words: Block copolymers, hydrogel, self-assembly

INTRODUCTION

Supramolecular assembly represents a dynamic tool for the fabrication of substantial functional complex architectures.[1-3] The primary driving force for building self-assembled objects arises from the capacity of small and discrete entities to assemble spontaneously into more organized systems.[4,5]Among the variety of self-assembled polymer architectures that are routinely utilized,[6] linear block copolymers (BCPs) unequivocally play an eminent multifaceted role in nanoscience.[7] Self-assembly of amphiphilic BCPs in aqueous solution is an inexpensive bottom-up strategy to create new polymeric nanostructures with seemingly endless possibilities in biomedical applications.[8,9]

A control over the self-assembly of amphiphilic BCPs typically relies on the volume fraction or ratio of hydrophobic and hydrophilic blocks along with their chain topology and architecture.[10] The unfavorable contact between water and the hydrophobic segments results in their self-assembly into small aggregates, which exhibit a rich polymorphism, the simplest structure being spherical micelles.[5] Micelles can emerge into flexible and elongated aggregates, referred to as worm-like micelles (WLMs).[11] As a result of their transient nature, WLMs display unprecedented dynamic and static properties which are exploited in numerous fields.[12]

The course of cutaneous wound healing is immensely complex, controlled by an intricate interplay between factors

Address for correspondence:
Dr. Monalisa Mukherjee,
Amity Institute of Click Chemistry Research and Studies,
J3 Block, Lab 103, Amity University, Noida, Uttar Pradesh, India.
E-mail: mmukherjee@amity.edu

Access this article online

Quick Response Code:

Website: www.japtr.org

DOI: 10.4103/japtr.JAPTR_153_19

How to cite this article: Singh A, Shakeel A, Kochhar D, Jeevanandham S, Rajput SK, Mukherjee M. Polymeric worm-like nanomicellar system for accelerated wound healing. J Adv Pharm Technol Res 2020;11:36-43.

operating in concert to reinstate injured skin.[13] This process occurs with the intricate reorganization of extracellular matrix networks.[14] Owing to this convoluted repair system, normal wound healing can only support a maladaptive regeneration of human skin.[15,16] Among biomaterials utilized as wound dressings, polymer-based sponges are ideal candidates for wound dressings.[17] Herein, with a suite of characterizations, we delineate the mechanism behind the formation of spherical and WLMs from poly(DEAEMA-co-AAc) (PDEA) self-assembly which demonstrates excellent accelerated cutaneous wound healing owing to their exceptional biocompatibility and capacity to maintain homeostasis in an otherwise maladaptive healing system.

SUBJECTS AND METHODS

Materials

AAc (99% pure) was purchased from Qualigen fine chemicals, India. DEAEMA (98% pure) was acquired from Aldrich, USA. Synthesis and assays were carried out in triple deionized water.

Synthesis

The synthesis was done through free-radical aqueous copolymerization using DEAEMA (20 mol%), AAc (80 mol%), Ammonium persulphate (APS), and Tetramethylethylenediamine (TEMED) as reported earlier.[9] The monomer mixture was then poured into molds and kept in a water bath at 40°C for 20 h. The hydrogels were kept at −20°C overnight and lyophilized at −70°C for 48 h.

Characterization

The surface morphology of the synthesized PDEA sponges was studied through scanning electron microscopy (Zeiss EVO 50). Transmission electron microscopy (TEM) micrographs were taken on a JEOL, JEM-2100F electron microscope at an acceleration voltage of 200 kV. Fourier-transform infrared (FTIR) was performed on attenuated total reflection-FTIR (ATR-FTIR) model, Nicolet-5DX F fitted with a temperature control. The samples were characterized in the wavenumber range of 4000–500 cm^{-1} at a fixed resolution of 4 cm^{-1}. X-ray photoelectron spectroscopy (XPS) absorption measurements were done at BL-14 beamline of Indus 2 synchrotron radiation source, Indore. The rheology was studied by utilizing small-amplitude oscillatory shear experiments using a fixed stress of 1.0 Pa, on an AR 500 Rheometer (TA Instruments, Surrey, England). Atomic force microscope (AFM) image was obtained through a Nanoscope IIIa at IUAC, New Delhi with tapping mode.[3,5]

Swelling study

Lyophilized PDEA sponges were weighed (Wo) and kept in phosphate-buffered saline (PBS) solution of pH (7.4) at room temperature. The samples were removed at fixed intervals of time, and the swollen weight (W_t) was recorded till equilibrium was attained.[3]

The equilibrium ratio at a particular time *t* was calculated as:

$$ESR(\%) = \frac{Wt - W0}{W0} \times 100$$

Where,

W_0 = Initial dry sample weight

W_t = Final swollen sample weight

In vitro release study

PDEA sponges were immersed in benzalkonium chloride (BZC) solution prepared in PBS (1 mg/ml) till equilibrium swelling was attained. The loaded sponges were then dried and immersed in fresh PBS, and the system was kept in a shaker incubator at 75 rpm. At a fixed time interval, 2 ml of the aliquot was withdrawn from solution. The concentration of BZC released from the hydrogel was determined at 262 nm by an ultraviolet–visible spectrophotometer in triplicates.[3,5]

Cell viability assay

The prepared sponge extract obtained after incubation at 37°C for 48 h (200 µl per well in triplicates) was added to tissue culture plates (Corning). Human dermal fibroblast α (HDFα) cells were trypsinized, and the cell density was determined using a hemocytometer, and 200 µl/well of cell suspension (~3000 cells) were added to the sponge extract. After 48 h of incubation, cytotoxicity was assessed using 3-(4,5-Dimethylthiazol-2-yl)-2,5-diphenyltetrazolium bromide (ThermoFisher). The readings were taken using enzyme-linked immunosorbent assay (ELISA) plate reader at 570 nm after 4 h incubation.[3,5]

$$\text{Cellviability}(\%) = \frac{\text{Absorbanceoftest} - \text{Absorbanceofblank}}{\text{Absorbanceofcontrol} - \text{Absorbanceofblank}} \times 100$$

T-test was used to perform statistical analysis. $P < 0.05$ was considered statistically significant.

Experimental protocol for evaluation of wound healing

Experimental design

Animals for the present investigation were approved by the Institutional Animal Ethical Committee, Amity University, Noida as per the guidelines of CPCSEA, New Delhi, India.

Wistar albino rats of either sex (weight 180–200 g) were allocated into two groups (normal control and treatment group having 6 rats/group). The control group was subjected to normal healing, whereas the treatment group received topical application of PDEA sponges (0.5 mg) swollen in normal saline (1 ml) over a circular area of 10 mm diameter was applied daily.

Creation of wound

The dorsal area of all animals was cleaned by trimming their hair and rinsed with 10% povidone-iodine solution, followed by 70% isopropyl alcohol. Animals were anesthetized by intraperitoneal injection of xylazine (10 mg/kg) and ketamine hydrochloride (25 mg/kg). A full-thickness excisional wound was created by biopsy punch (diameter = 10 mm; AccuPunch, Acuderm, USA).[3]

Measurement of wound contraction and epithelization period

In the excision wound model, the wound area was measured by tracing the wound with the help of a transparent sheet using millimeter-based graph paper at different time points including 0, 4th, and 10th day for both groups. Wound contraction was calculated:[3]

$$\%\text{woundcontraction} = \frac{\text{Initialwoundarea} - \text{specificdaywoundarea}}{\text{Initialwoundarea}} \times 100$$

Assessment of immunological parameters

The estimation of various immunological biomarkers was carried by measuring interleukin-6 (IL-6), IL-10, and tumor necrosis factor-alpha (TNF-α) for the estimation of inflammatory cytokines using ELISA kits (Raybiotec, USA). Blood sample was collected from each animal, and serum was separated by centrifugation at 3,000 RPM for 10 min. All the biochemical estimations were done on fresh tissue samples.

Histological assessment

Histological assessment was done at an alternative time point (4th day and 10th day). Wounds were removed under euthanasia by intraperitoneal injection of pentobarbital (200 mg). Animals from each group were sacrificed. Wound skins were taken for routine processing and H and E staining (fixating, dehydrating, embedding, and cutting). Slides were analyzed under light microscope (COSLAB, INDIA).

RESULTS AND DISCUSSION

Morphological characterizations

Cross-sectional morphology of the as-synthesised PDEAsponges indicates that the interior of the gels is uniformly macroporous at pH 7.4. PDEA exhibited a large average pore size primarily owing to the ionization of AAc units [Figure 1a-c]. The PAAc chains undergo dissociation facilitated by the ionization of the pendant groups which give rise to an electrostatic repulsion causing the network to swell. The amount of water entrapped within the polymer matrix directly corresponds to the pore size retrieved upon swelling. The greater the amount of water entrapped between the polymer networks, the larger will be the pore size obtained upon lyophilization of the swollen gel. Thus, increasing AAc content increases the average pore size of the PDEA at pH 7.4 producing sponge-like PDEA with enhanced wound exudate absorption and moisture vapor transmission.

The self-assembling nature of amphiphilic polymers facilitates the formation of a range of micellar morphologies attributed to two competing factors: interfacial energy between the two blocks and chain stretching.[18] Conspicuous from the TEM images [Figure 2a], micelles of varying sizes were observed due to the emergence of aggregates by the amphiphilic polymeric structures. As a consequence of the asymmetric diblock, an energetically favorable micellar morphology is obtained wherein poly(DEAEMA-co-AAc) hydrophobic blocks prefer to aggregate into spherical microdomains leaving pAAc to surround them as "coronas" [Figure 2b and c] These individual monodisperse spherical micelles [Figure 2b and c] can be considered as the starting morphology for various aggregates, insisting the nonergodic nature of copolymer amphiphiles.[19] On further investigation of the crystalline domains of [Figure 2c], we observed a d-spacing of 0.159 [Figure 2d], whereas the Selected area electron diffraction (SAED) patterns reveal planes of (205), (201), (301), and (111) [Figure 2e].

Intramolecular self-collapsing varies with polymeric chain flexibility bolstering interfacial collision of these amphiphilic blocks. The imbalance in the volume fraction of PDEA copolymer assembly is majorly due to thermodynamic instability with predominant hydrophilic domains at the corona which are superseded by the hydrophobic interactions between the cores ultimately leading to the morphological transition of micelles minimizing the entropy. Subsequently, the increase in the

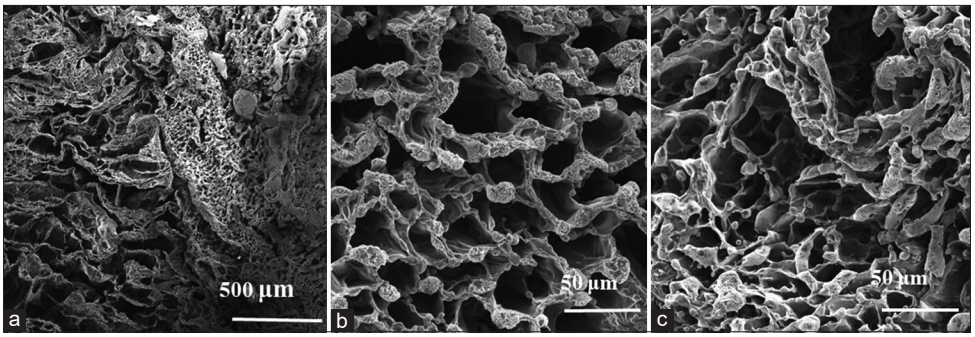

Figure 1: Scanning electron microscopy a photomicrographs of the poly (DEAEMA-co-AAc) (a-c) Displays uniformly distributed pores

degree of quaternization of highly cross-linked DEAEMA blocks triggers self-collapse of micellar morphology eventually resulting in the profusion of WLMs.[20] These elongated WLMs are energetically favorable relative to shortened cylinders with incorporated end defects, since these structures allow uniform curvature across the entire aggregate. Above a concentration threshold, the WLMs entangle into a dynamic reversible network [Figure 2f] that is constantly breaking and reforming.

The surface morphology of PDEA micelles was investigated using AFM. Few isolated domains from the topologically flat surface resembled the micellar architectures of PDEA copolymers with low surface energy [Figure 3a]. AFM images show the spherical structures with a maximum height profile of 13.69 nm, slightly larger than the thickness of ~6.2 nm [Figure 3b], confirming the formation of spherical polymeric micelles. The spongy nature of PDEA micelles can be correlated with the dot-like disordered microdomains oriented parallel to the substrate. The low average surface roughness of 1.04 nm affirms the smooth and homogenous morphology of PDEA micelles [Figure 3c].

Chemical characterizations

The structural aspects of PDEA BCPs are investigated using ATR-FTIR spectroscopy [Figure 4]. The broad and intense peak at 3448 cm^{-1} is attributed to intermolecular hydrogen bonding and the dimerization of saturated aliphatic acid (PAAc) groups in the polymer matrices.[21] The sharp and intense peaks at 2925 cm^{-1} and 2853 cm^{-1} correspond to the strong asymmetrical and symmetrical stretching vibrations of methylene groups in the copolymer blocks, respectively. However, a prominent asymmetrical stretching band at 1639 cm^{-1} is attributed to dominant carboxylate anions (COO-) of PAAc domains supporting the polyelectrolyte complexation. The characteristic peak at 1165 cm^{-1} is ascribed to the symmetrical C-N-C (tertiary aliphatic amine) stretching of PDEAEMA pendant groups confirming their quaternization effect leading to strong electrolytic complexation of PDEA blocks.[5]

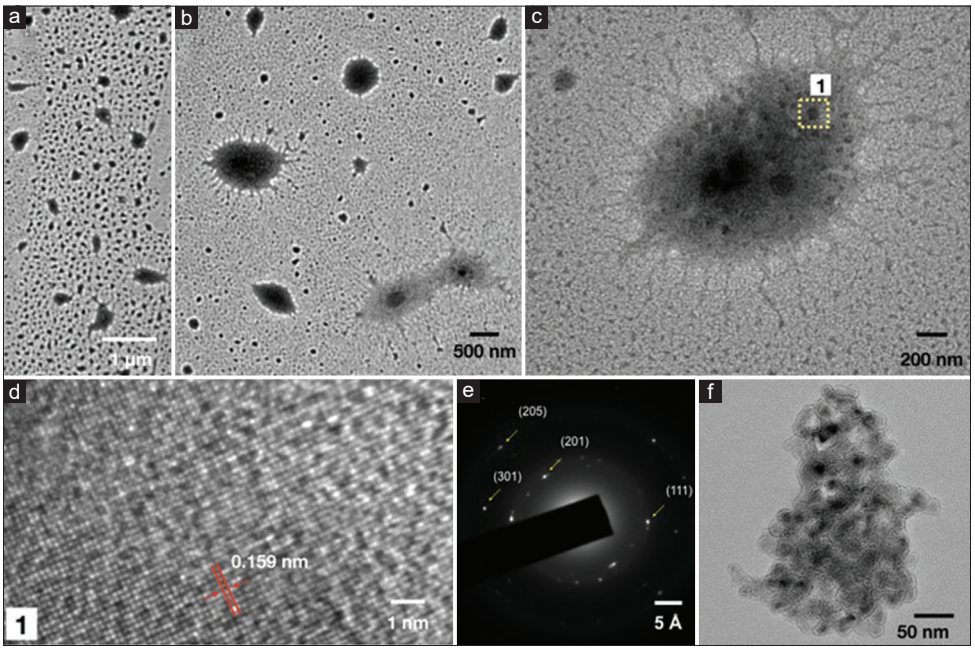

Figure 2: (a-c) Transmission electron microscopy micrographs displaying centrosymmetric core-shell polymeric micelles. (d) Crystalline domains of Part c. (e) SAED pattern corresponding to Part d. (f) dynamic networks of worm like micelles

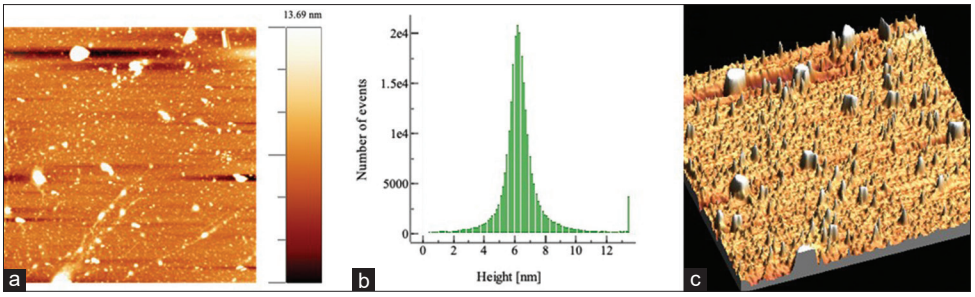

Figure 3: Atomic force microscope displaying surface topography of poly (DEAEMA-co-AAc) sponges. (a) Atomic force microscope height image with corresponding histogram. (b) corresponding height profile. (c) Three-dimensional representation

The wide-scan XPS survey peaks encompass the existence of C 1s, N1s, and O1s components at 286.2 eV, 401.7 eV, and 532.7 eV, respectively [Figure 5a]. The high-resolution C1s spectrum [Figure 5b] of PDEA can be deconvoluted into four peaks, positioned at the binding energies of 284.6 eV (C=C), 285.8 eV (C-C/C-H), 287 eV (C-N/C-O), and 288.7 eV (O-C=O). The dominant C-C/C-H peaks correspond to the aliphatic carbon atoms of the long polymer backbone. However, the broad peaks of the O-C = O component affirm the presence of secondary carbon atoms of the ester groups of PDEAEMA. Meanwhile, the intensified C-N/C-O peaks represent the presence of few neutral moieties in PDEAEMA endeavoring strong electrolytic interactions with COO moieties of PAAc. Moreover, the sharp O1s spectrum of the BCP can be fitted into three Gaussian peaks centered at 531.3 eV (C = O), 532.7 eV (O-H), and 534.2 eV (C-O-C) [Figure 5c]. The predominance of C = O over C-O-C moieties confirms the entanglement of PAAc domains at the corona of polymeric micelles surrounding the hydrophobic core DEAEMA domains. Furthermore, the intensified O-H peaks arises as a consequence of intermolecular hydrogen bonding, and plausible dimerization of PAAc domains with water molecules.[5] In addition, the N1s spectrum can also be deconvoluted into two distinct broad peaks representing significant XPS signals at 400.2 eV corresponding to neutral C-N moieties, whereas the other characteristic peak at 402.6 eV affirms the quaternization (C-N +) effect of the hydrophobic domains resulting in the formation of polyelectrolyte complexes [Figure 5d].

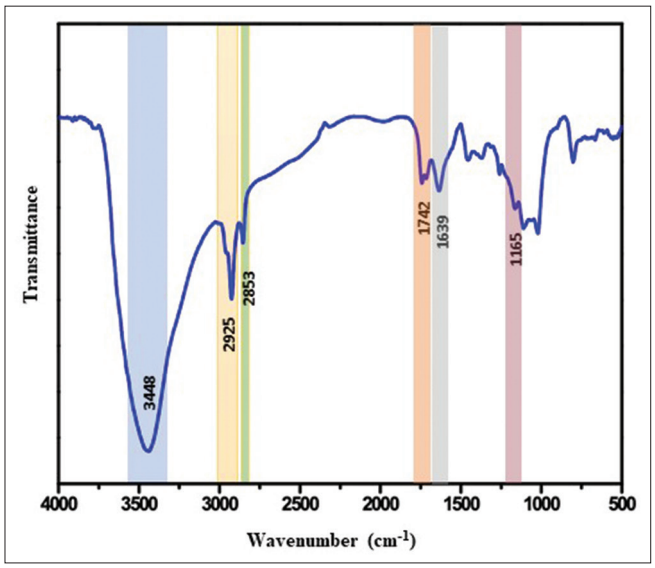

Figure 4: Fourier-transform infrared of poly (DEAEMA-co-AAc) sponges

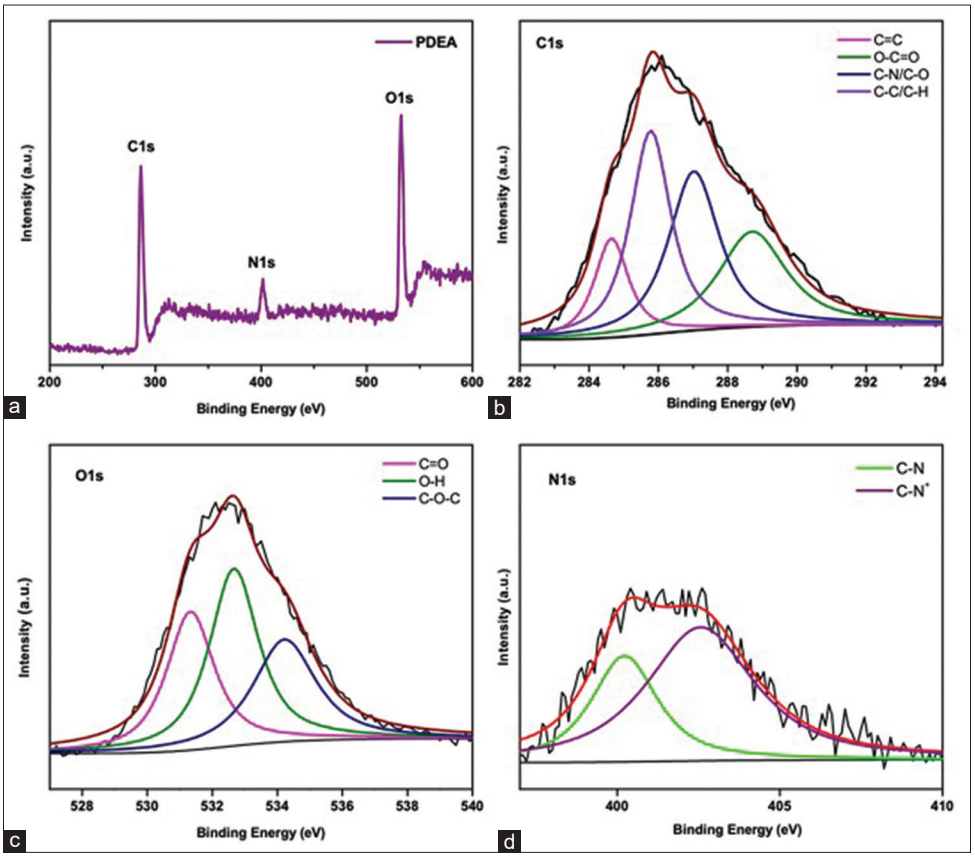

Figure 5: X-ray photoelectron studies of poly (DEAEMA-co-AAc) sponges. (a) Survey spectrum. (b) high-resolution C1s spectrum. (c) High-resolution O1s spectrum. (d) High-resolution N1s spectrum

Rheology

The rheology pattern in Figure 6 shows the typical plots of shear storage (G′) and loss (G′′) modulus versus the oscillatory frequency (ω) sweep curves. The results of frequency sweep experiments the relation G′(ω) > G′′(ω), indicating spongy-like stable elastic behavior of PDEA gels. The calculated loss factor tan δ (G′′/G′) showing a substantial increase in values 0.1–0.16 (Gradual increase in temperature) indicates higher energy dissipation of PDEA sponges resulting slightly viscous nature to the material.

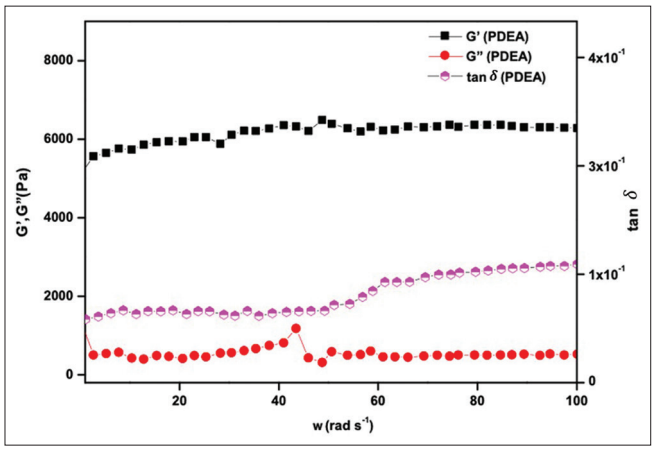

Figure 6: Rheology of poly (DEAEMA-co-AAc) sponges

Swelling and release studies

When kept in PBS buffer of pH 7.4, the sponges initially showed fast swelling for the first 15 h and attained the equilibrium swelling after ~28H with an equilibrium swelling ratio of ~3200% [Figure 7a]. The –COOH groups of AAc bound to the polymeric chain becomes protonated forming –COO^- ions. The electrostatic repulsions between the –COO^- lead to the swelling of PDEA sponge network forming large pores.[22]

The drug-loaded hydrogel membranes followed a two-stage drug release profile as shown in [Figure 7b]. At physiological pH (7.4), the electrostatic repulsion between the carboxylate anions causes the network to swell and allows the entrapped drug to move outside the matrix through osmosis. The slow and extended swelling property leads to sustained release of drug with an exponential increase in concentration till ~ 25H releasing 88% of the drug.

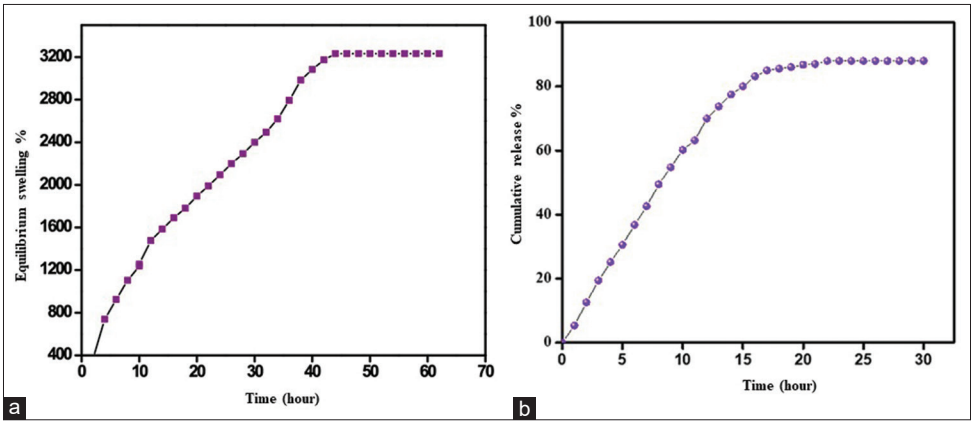

Figure 7: (a) Equilibrium swelling capacity of hydrogel nanomembrane around 3200%. (b) Cumulative drug release up to 88%

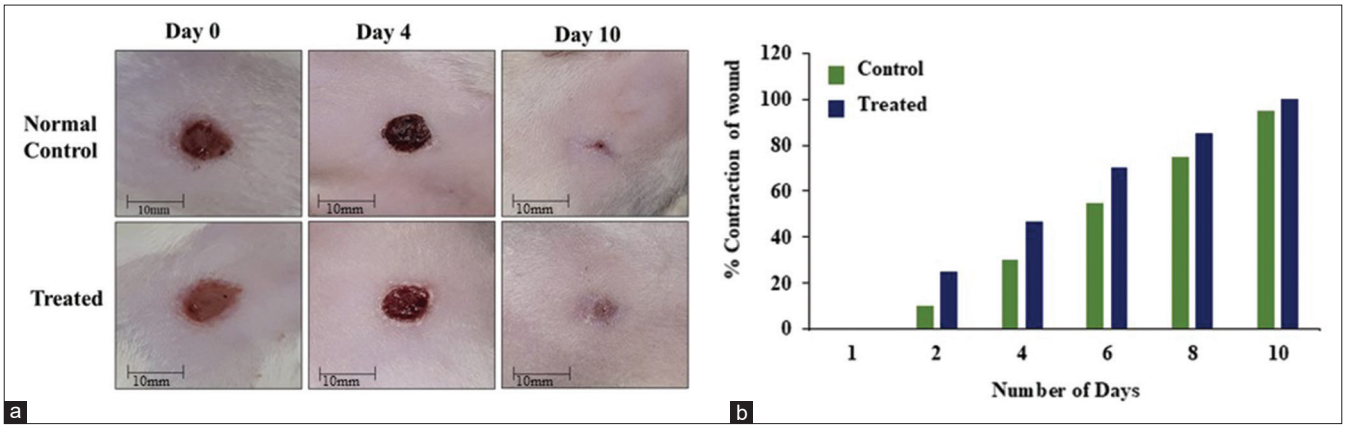

Figure 8: (a) *In vivo* assessment of wound healing on Wistar rat at day 0, 4, and 10 with normal control and treated groups (scale bar 10 mm) with graphical representation of (b) wound contraction percentage

Wound healing

Percentage of wound contraction and healing rate

In the treated group, the healing rate of the wound on the 4th day [Figure 8b] was greater than the control (50% and 30%, respectively). On the 10th day, complete wound closure was observed in the treated rats, whereas only 70% recovery was seen in the normal control [Figure 8a]. Moreover, no fester or hypertrophic scarring was observed at the wound site in the treated rats and the fur started to reappear by the 10th day.

Histological assessment

The early phase (4th day) shows an increased level of polymorphonuclear leukocytes, polymorphonuclear neutrophils, or inflammatory cells near the excision line of the wound. The demarcation line showed the complete separation of exudate formation, and the continuous layer of epithelial cells was absent. However, in the control group, higher exudate accumulation was observed which reflects the deposition of a foreign substance and can be measured by increase leukocytes infiltration. The absence of exudates formation and lower level of leukocytes infiltration at later phase indicated that the upsurge of inflammatory cytokines release was almost finished. In addition, in comparison to normal control, a complete layer of epithelialization was observed in treated animals on the 10th day which corroborates the intense healing of the wound. Collagen deposition was significantly raised at the end of healing of the wound in treated animals. Less deposition of collagen indicated incomplete wound healing in normal control animals compared to the treated group [Figure 9].

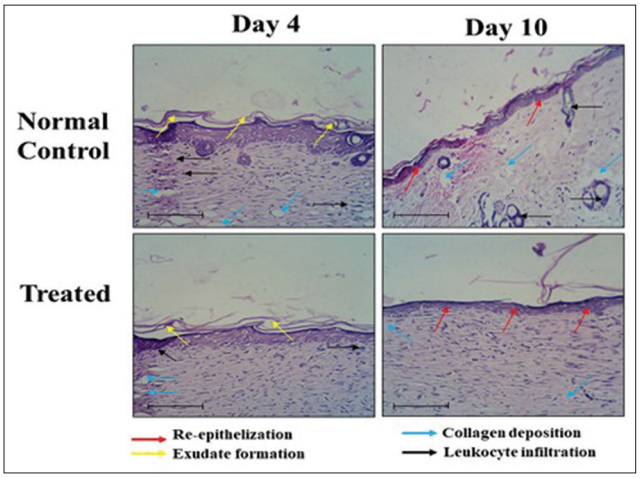

Figure 9: Histological assessment of wounds at day 4 and day 10

Early re-epithelialization observed in the treated rats as compared to control was validated by the significant reduction in the concentration of IL-6 and TNF-α, and an increase in IL-10 [Figure 10] unveiling the anti-inflammatory potential of the PDEA sponges.

CONCLUSIONS

In summary, our findings delineate the intimate interaction between amphiphilic BCPs to achieve hierarchical structures that facilitate accelerated wound healing by decreasing oxygen tension, promoting wound dehydration, and reducing inflammation. Experimental procedures for the on-demand synthesis of hydrogels are undertaken after carefully setting the properties desired to attain spherical and worm-like nanomicellar structures having vital implications on their morphological and chemical characteristics as well as their biocompatibility, swelling and release, and wound healing properties, making them competitive candidates to be applied as potent wound dressings.

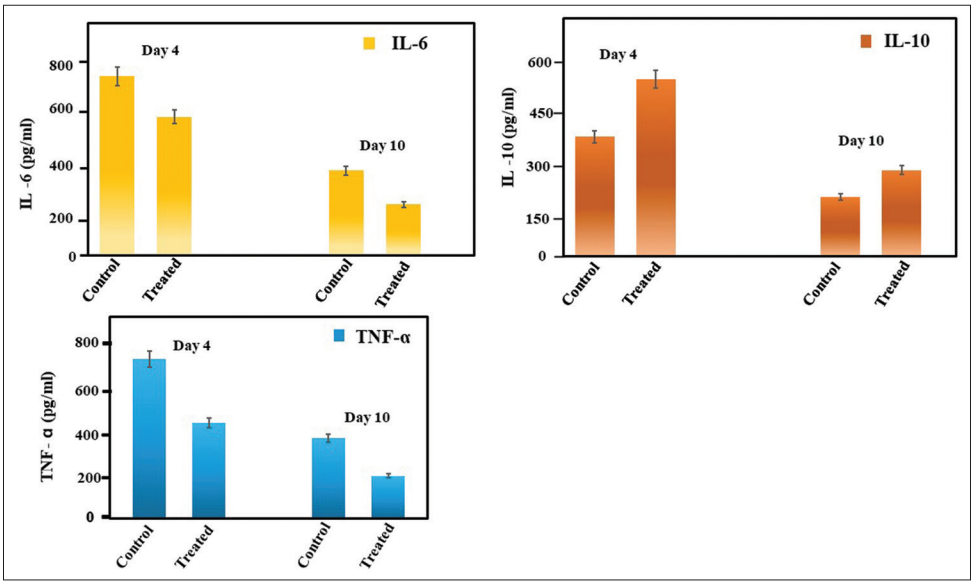

Figure 10: Quantification of IL-6, TNFα, and IL-10

Financial support and sponsorship

Prof. Monalisa Mukherjee thanks the Department of Biotechnology BT/PR21866/NNT/28/1145/2016 for funding this project, and Amity University Uttar Pradesh Noida for providing research infrastructure.

Conflicts of interest

There are no conflicts of interest.

REFERENCES

1. Lehn JM. Toward self-organization and complex matter. Science 2002;295:2400-3.
2. Whitesides GM, Boncheva M. Beyond molecules: Self-assembly of mesoscopic and macroscopic components. Proc Natl Acad Sci U S A 2002;99:4769-74.
3. Singh A, Bhattacharya R, Shakeel A, Sharma AK, Jeevanandham S, Kumar A, *et al*. Hydrogel nanotubes with ice helices as exotic nanostructures for diabetic wound healing. Mater Horiz 2019;6:274-84.
4. Lehn JM. Perspectives in supramolecular chemistry-from molecular recognition towards molecular information processing and self-organization. Angew Chem Int Ed Engl 1990;29:1304-19.
5. Shakeel A, Bhattacharya R, Jeevanandham S, Kochhar D, Singh A, Mehra L, *et al*. Graphene quantum dots in the game of directing polymer self-assembly to exotic kagome lattice and janus nanostructures. ACS Nano 2019;13:9397-407.
6. Bates CM, Bates FS. 50th anniversary perspective: Block polymers-pure potential. Macromolecules 2017;50:3-22.
7. Giacomelli C, Schmidt V, Aissou K, Borsali R. Block copolymer systems: From single chain to self-assembled nanostructures. Langmuir 2010;26:15734-44.
8. Elsabahy M, Wooley KL. Design of polymeric nanoparticles for biomedical delivery applications. Chem Soc Rev 2012;41:2545-61.
9. Suhag D, Bhatia R, Das S, Shakeel A, Ghosh A, Singh A, *et al*. Physically cross-linked pH-responsive hydrogels with tunable formulations for controlled drug delivery. RSC Adv 2015;5:53963-72.
10. Zhang L, Eisenberg A. Formation of crew-cut aggregates of various morphologies from amphiphilic block copolymers in solution. Polym. Adv. Technol 1998;11:677-99.
11. Dreiss CA. Wormlike micelles: Where do we stand? Recent developments, linear rheology and scattering techniques. Soft Matter 2007;3:956-70.
12. Yang J. Viscoelastic wormlike micelles and their applications. Curr Opin Colloid Interface Sci 2002;7:276-81.
13. Chantre CO, Hoerstrup SP, Parker KK. Engineering biomimetic and instructive materials for wound healing and regeneration. Curr. Opin. Biomed. Eng 2019;10:97-106.
14. Martin P. Wound healing-aiming for perfect skin regeneration. Science 1997;276:75-81.
15. Han G, Ceilley R. Chronic wound healing: A review of current management and treatments. Adv Ther 2017;34:599-610.
16. Wang SY, Kim H, Kwak G, Yoon HY, Jo SD, Lee JE, *et al*. Development of biocompatible HA hydrogels embedded with a new synthetic peptide promoting cellular migration for advanced wound care management. Adv Sci (Weinh) 2018;5:1800852.
17. García MC, Aldana AA, Tártara LI, Alovero F, Strumia MC, Manzo RH, *et al*. Bioadhesive and biocompatible films as wound dressing materials based on a novel dendronized chitosan loaded with ciprofloxacin. Carbohydr Polym 2017;175:75-86.
18. Mai Y, Eisenberg A. Self-assembly of block copolymers. Chem Soc Rev 2012;41:5969-85.
19. Blanazs A, Armes SP, Ryan AJ. Self-assembled block copolymer aggregates: From micelles to vesicles and their biological applications. Macromol Rapid Commun 2009;30:267-77.
20. Thanneeru S, Li W, He J. Controllable self-assembly of amphiphilic tadpole-shaped polymer single-chain nanoparticles prepared through intrachain photo-cross-linking. Langmuir 2019;35:2619-29.
21. Todica M, Stefan R, Pop CV, Olar L. IR and Raman investigation of some poly (acrylic) acid gels in aqueous and Neutralized State. Acta Phys. Pol 2015;1:128-35.
22. Torres MT, Peppas NA. Molecular design and *in vitro* studies of novel pH-sensitive hydrogels for the oral delivery of calcitonin. Macromolecules 1999;32:6646-51.